SCIENCE CHINA
Life Sciences

•RESEARCH PAPER•

September 2020 Vol.63 No.9: 1337–1346
https://doi.org/10.1007/s11427-019-1567-0

BDNF improves axon transportation and rescues visual function in a rodent model of acute elevation of intraocular pressure

Rui Du[1], Xu Wang[1] & Shigang He[1,2,3*]

[1]*School of Biomedical Engineering, Shanghai Jiao Tong University, Shanghai 200240, China;*
[2]*Institute of Natural Sciences, Shanghai Jiao Tong University, Shanghai 200240, China;*
[3]*Bio-X Institute, Shanghai Jiao Tong University, Shanghai 200240, China*

Received July 8, 2019; accepted September 28, 2019; published online March 16, 2020

Optic neuropathies lead to blindness; the common pathology is the degeneration of axons of the retinal ganglion cells. In this study, we used a rat model of retinal ischemia-reperfusion and a one-time intravitreal brain-derived neurotrophic factor (BDNF) injection; then we examined axon transportation function, continuity, physical presence of axons in different part of the optic nerve, and the expression level of proteins involved in axon transportation. We found that in the disease model, axon transportation was the most severely affected, followed by axon continuity, then the number of axons in the distal and proximal optic nerve. BDNF treatment relieved all reductions and significantly restored function. The molecular changes were more minor, probably due to massive gliosis of the optic nerve, so interpretation of protein expression data should be done with some caution. The process in this acute model resembles a fast-forward of changes in the chronic model of glaucoma. Therefore, impairment in axon transportation appears to be a common early process underlying different optic neuropathies. This research on effective intervention can be used to develop interventions for all optic neuropathies targeting axon transportation.

acute elevation of IOP, axon transportation, axon continuity, visual acuity, contrast sensitivity, rat

Citation: Du, R., Wang, X., and He, S. (2020). BDNF improves axon transportation and rescues visual function in a rodent model of acute elevation of intraocular pressure. Sci China Life Sci 63, 1337–1346. https://doi.org/10.1007/s11427-019-1567-0

INTRODUCTION

Optic neuropathy is a spectrum of diseases with optic nerve degeneration as a common pathology. The most prevalent optic neuropathy is glaucoma (Quigley et al., 1982; Weinreb et al., 2014; Yohannan and Boland, 2017; Xin et al., 2018; Huang et al., 2019; Liu et al., 2019; Qiao et al., 2019). However, optic nerve ischemia (Biousse and Newman, 2014; Patel and Margo, 2017), Leber's hereditary optic neuropathy (LHON) (Wallace et al., 1988; Huoponen et al., 1991; Johns et al., 1992; Sadun et al., 2000; Zhang et al., 2019) and autosomal dominant optic neuropathy (ADON) (Hoyt, 1980; Votruba et al., 1998; Alexander et al., 2000; Delettre et al., 2000) also exhibit optic nerve degeneration.

In a transgenic mouse line (Buckingham et al., 2008) with chronically elevated intraocular pressure (IOP), both axon transport function and continuity were impaired. However, losing continuity lagged behind the impairment of axon transport function by about 6 months. This work suggested a time window during which the restoration of axon transport may prevent loss of connectivity and visual function.

In previous work (Ren et al., 2012), we showed that BDNF gene or protein therapy could significantly rescue the number of ganglion cells capable of retrogradely transporting Flurogold (FG) and significantly improve visual function. In this study, we used a model of acute elevation of the IOP (Ren et al., 2012) to further examine the number of axons physically present at different parts of the optic nerve. We

*Corresponding author (email: shiganghe@sjtu.edu.cn)

also investigated changing expression levels of molecules responsible for axon transportation. We hope to explore common early mechanisms underlying axon degeneration in chronic and acute elevation of the IOP, as seen in glaucoma and optic nerve ischemia. If these mechanisms are also shared in LHON and ADON, intervention for all optic neuropathies could be envisioned.

RESULTS

BDNF treatment alleviates deficits of visual function in an acute IOP elevation model

In our previous work, we showed that BDNF gene therapy, BDNF protein treatments, and combination therapies all effectively stopped the decrease in the number of FG-labeled RGCs and the deterioration of visual function induced by acute elevation of IOP (Ren et al., 2012). BDNF gene therapy supplemented with BDNF protein treatment achieved the best effects. To focus on the rescuing effect of BDNF and to explore the mechanism behind it, we simplified the protocol to a single BDNF protein treatment for the acute elevation of IOP model in this study.

We verified the therapeutic effects by using a BNDF intraocular injection. BDNF was administered 6 h after a 45 min elevation of IOP. In the disease model without treatment, the visual acuity decreased to (52.1±2.1)%, (25.0 ±0.0)%, and (14.6±2.1)%; and the contrast detection threshold increased to (162.1±3.5)%, (186.2±0.0)%, and (206.9±0.0)% at the end of 3rd, 6th, and 9th week, respectively (Figure 1). A single intraocular administration of BDNF protein treatment alleviated the deficits of visual function; visual acuity recovered to (87.5±0.0)%, (62.5 ±0.0)%, and (60.4±1.4)%; and contrast detection threshold recovered to (122.4±1.7)%, (124.1±0.0)%, and (127.6 ±2.3)% at the corresponding time points (Figure 1). The detailed measurements of visual function were shown in Figure S1 in Supporting Information. These data were consistent with our previous study.

Disruption of axon transportation preceded axon discontinuity

We co-injected FG and DiD into the superior colliculus (SC) to evaluate the retrograde transport function (FG) and the axon continuity (DiD) 7 days before sacrificing the animals. The number of FG-positive RGCs decreased to (59.8±1.1)%, (43.3±1.6)%, and (22.8±1.3)%; and DiD-positive RGCs decreased to (73.5±1.3)%, (55.8±2.7)%, and (31.2±2.6)% of the control level at the end of 3rd, 6th, and 9th week, respectively (Figure 2). There is a larger reduction in the number of FG-positive RGCs than the DiD-positive RGCs, indicating that transport functions were compromised in many continuous axons. With BDNF protein administration, the reduction of both FG- and DiD-positive RGCs was reduced, reaching a level of (74.5±1.7)%, (68.7±1.4)%, and (64.9±1.4)% of the control for FG-positive and (84.6±2.5)%, (78.2±1.3)%, and (72.4±1.4)% for DiD-positive RGCs for corresponding time points (Figure 2). Again, the DiD-positive RGCs outnumbered the FG-positive ones in every case, suggesting that improving axon transportation help to maintain axon continuity.

We examined the change in anterograde transport function. First, we determined the minimal time for the dye to cover the entire SC uniformly. The fact that the continuous axons (DiD-positive) outnumbered the transporting axons (FG-positive) is an indication that the speed or the efficiency of the axon transportation were compromised, therefore a delay

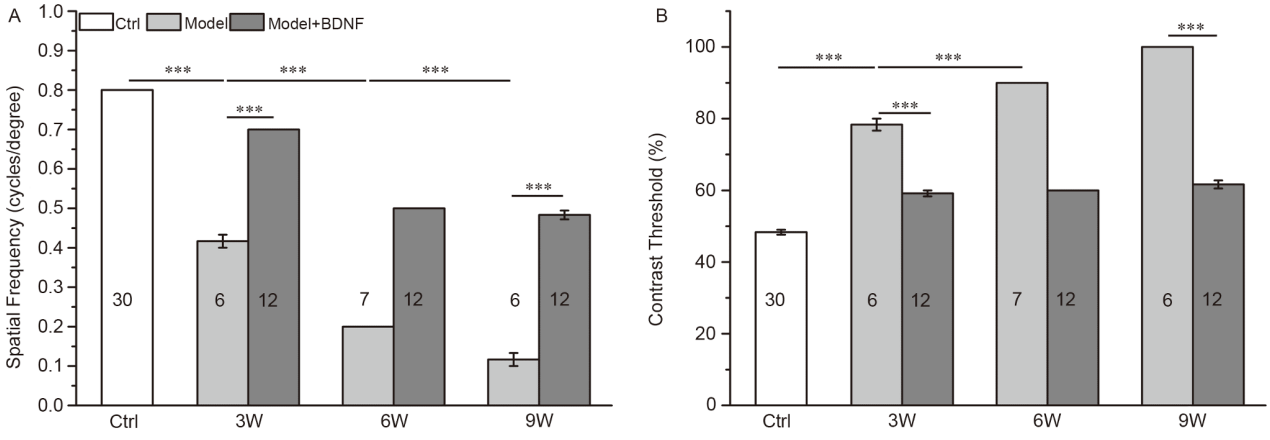

Figure 1 Behavioral test of visual function in the acute elevated IOP and BDNF treatment group. A, Visual acuity is measured when the water visual task correct rate is above 70%. The maximum spatial frequency decreased from 0.80 cpd (ctrl) to 0.12±0.02 cpd (9th week after elevated IOP). The BDNF was able to rescue some function, to 0.48±0.01 cpd at 9th week after elevated IOP. B, The contrast threshold is measured when the water visual task correct rate above 70%. The minimum contrast threshold increased from (48.3±0.7)% (ctrl) to (100.0±0.0)% (9th week after elevated IOP). The BDNF rescued some function to (61.7±1.1)% at 9th week after elevated IOP. 3W: 3rd week, 6W: 6th week, 9W: 9th week. cpd: cycle per degree. ***, P<0.001.

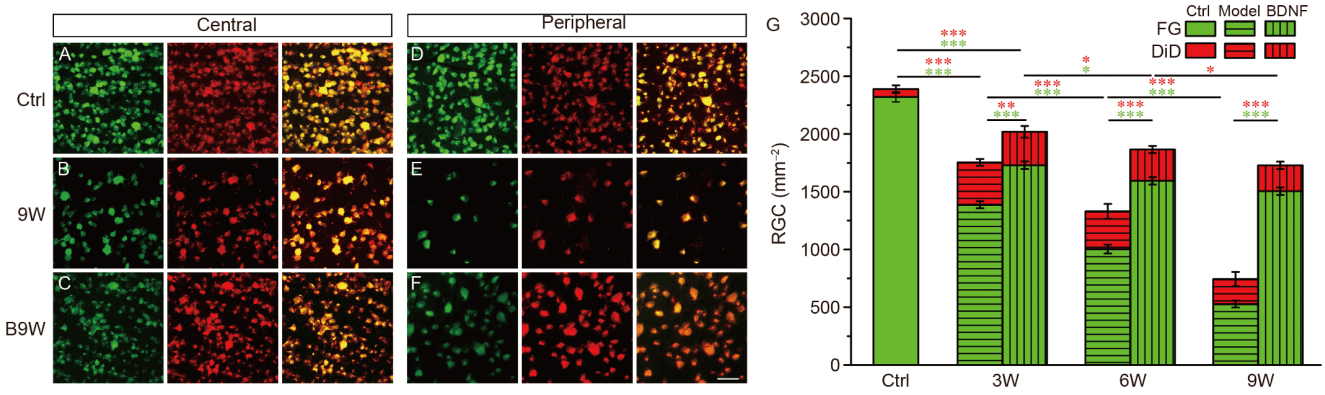

Figure 2 RGCs retrogradely labeled with FG and DiD. RGCs retrogradely labeled with FG and DiD of control (A), experimental (B) and BDNF-treated experimental (C) animals in the central retina at 9th week after elevated IOP. FG- and DiD-labeled RGCs of control (D), experimental (E), and BDNF-treated experimental (F) animals in the peripheral retina at 9th week after elevated IOP. Density of double labeled RGCs at each time point (G). Scale bar: 50 μm; *, $P<0.05$, **, $P<0.01$, ***, $P<0.001$.

in observation may have reduced the sensitivity of the measurements. The 3D reconstruction from serial coronal sections showed that it took 6 h for the dye to reach and partially cover the SC and 12 h to cover the entire SC uniformly in the controls. The difference between 12 and 24 h delay was largely in the pixel intensity (Figure S2 in Supporting Information). Therefore, we decided to examine the SC 12 h after intraocular dye injection.

In the 3D reconstructions (Figure 3), the percentage of CTB-positive pixels decreased to (68.6±2.0)%, (55.9±2.5)%, and (42.4±2.3)% of the control level at the end of 3rd, 6th, and 9th week after elevation of IOP, respectively. In the BDNF-treated group, the percent of CTB-positive pixels was (91.3±2.4)%, (75.7±1.1)%, and (70.6±1.1)%, as compared to controls, at the corresponding time points (Figure 3). These findings showed that anterograde transportation was impaired by acute elevation of the IOP and was remedied by the BDNF treatment.

Number of axons in the optic nerve

We quantified the number of axons in the semi-thin sections of the proximal part (close to the optic disc) and the distal part (close to the optic chiasm) of the optic nerve to confirm the physical presence of axons. The acute elevation of IOP induced a reduction in the number of axons in the proximal end of the optic nerve, to (92.5±0.7)%, (77.6 ±0.9)%, and (64.4±0.5)% of the control at the end of 3rd, 6th, and 9th week, respectively (Figure 4). The reduction in the distal end of the optic nerve was more pronounced, to (78.0±1.5)%, (65.2±1.4)%, and (50.4±1.3)%, for the corresponding time points (Figure 4B and D). A single administration of BDNF significantly deterred the loss of axons; the density of axons in the proximal end recovered to (92.5±0.7)%, (96.1±3.1)%, and (92.7±2.0)%, and in the distal end, recovered to (85.0±0.5)%, (78.9±1.3)%, and (80.6±1.7)% (Figure 4B–D) at the end of 3rd, 6th, and 9th week, respectively. In the preparations treated with BDNF, we also examined the axon density in the intermediate part of the optic nerve. The density of axons fell between the proximal end and the distal end, again supporting a retrograde degeneration (Figure S3 in Supporting Information).

Molecular changes underlying transportation function

To understand the molecular mechanism underlying the changes of axon transportation, we examined the level of proteins involved in axon transportation both in the retina and in the optic nerve using Western Blotting.

Dynein is a motor protein responsible for retrograde transportation. In the optic nerve, the level of dynein showed a significant decrease at the end of the 3rd week and a further significant decrease at the end of 6th week after the transient IOP elevation; levels remained stable thereafter (Figure 5A and C). In the retina, the dynein level began to exhibit significant decrease at the end of 6th week, and continued to the end of 9th week (Figure 5B and D). With BDNF treatment, the dynein level was restored both in the retina and in the optic nerve (Figure 5C and D).

Kinesin, a motor protein responsible for anterograde transportation, exhibited a significant reduction in the optic nerve at the end of the 3rd week, and remained stable thereafter (Figure 5A and E). In the retina, kinesin showed an increase that persisted from the end of the 3rd week to the 9th week (Figure 5B and F). BDNF reverted these changes to previous levels (Figure 5E and F).

The level of tubulin, the track for axon transportation, remained unchanged both in the retina and the optic nerve in all groups and at all times (Figure 5A, B, G, and H), except for a small increase in the optic nerve between model and treatment groups at the end of the 9th week (Figure 5G).

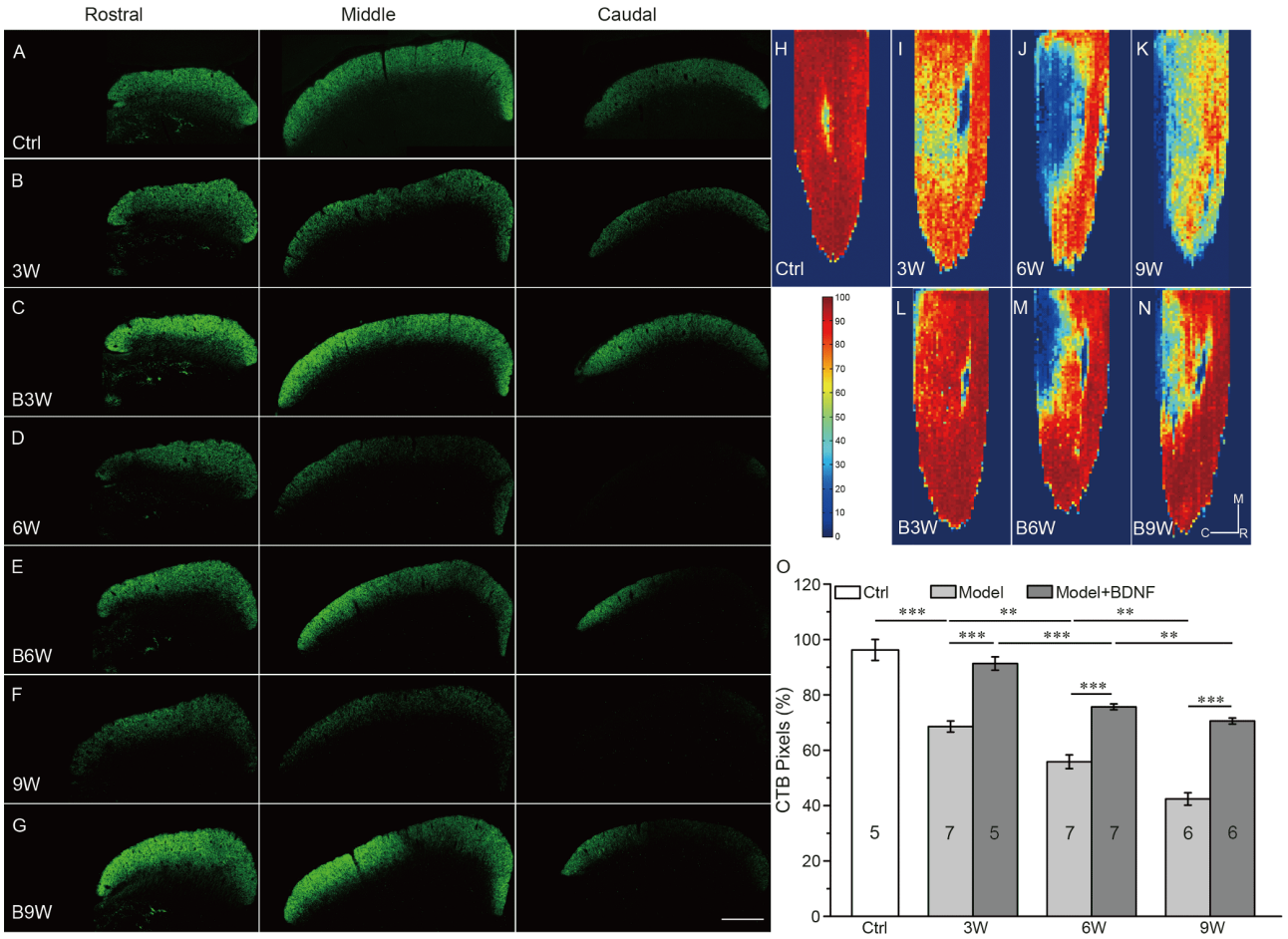

Figure 3 Anterograde transport in acute elevation of IOP and BDNF treatment groups. A–G, sections of the superior colliculus from rostral to caudal of each group. H–N, examples of the superior colliculus in each group. O, superior colliculus retinotopic map. Scale bar: 500 μm; *, $P<0.05$, **, $P<0.01$, ***, $P<0.001$.

However, neither model nor treatment was significantly different from the control group.

DISCUSSION

Improving axon transport function rescues visual function

We applied the co-labeling protocol of Buckingham (Buckingham et al., 2008) to a rat model of acute IOP elevation, and obtained similar results. The number of both continuous and transporting axons decreased, and the loss of transporting axons was much more pronounced at every time point observed. Our finding are consistent with previous results which suggest that in this model, the impairment of axon transportation also precedes disconnection (Buckingham et al., 2008; Ren et al., 2012; Wang et al., 2017; Zhou et al., 2017; Luan et al., 2018; Zhang et al., 2018; Xia et al., 2019).

Our quantification of axons in semi-thin sections showed an interesting trend when comparing number of axons in different experiments. The proximal end of the optic nerve contained more axons than the distal end, which in turn exceeded the number revealed by lipophilic DiD. Since the degeneration is retrograde, it is likely that the proximal nerve contains more axons than the distal portion. DiD is able to detect discontinuity at any part of the axon, and is therefore more sensitive than the actual number of axons at a certain section. Not all continuous axons are capable of transportation; the number of RGCs capable of transportation is most dramatically affected, results that also agree with previous work (Reichstein et al., 2007; Buckingham et al., 2008; Ren et al., 2012).

The sequence of changes suggests that impairment of axon transportation preceded the disruption of discontinuity during degeneration, and degeneration propagated from distal to proximal portion (Cavanagh, 1979; Coleman, 2005; Whitmore et al., 2005). In treated animals, rescue of axon transportation maintained axon integrity and visual function. Among all parameters, the change in the number of transporting axons is best correlated with the change in visual function, suggesting that the axons incapable of transportation stop contributing to visual function.

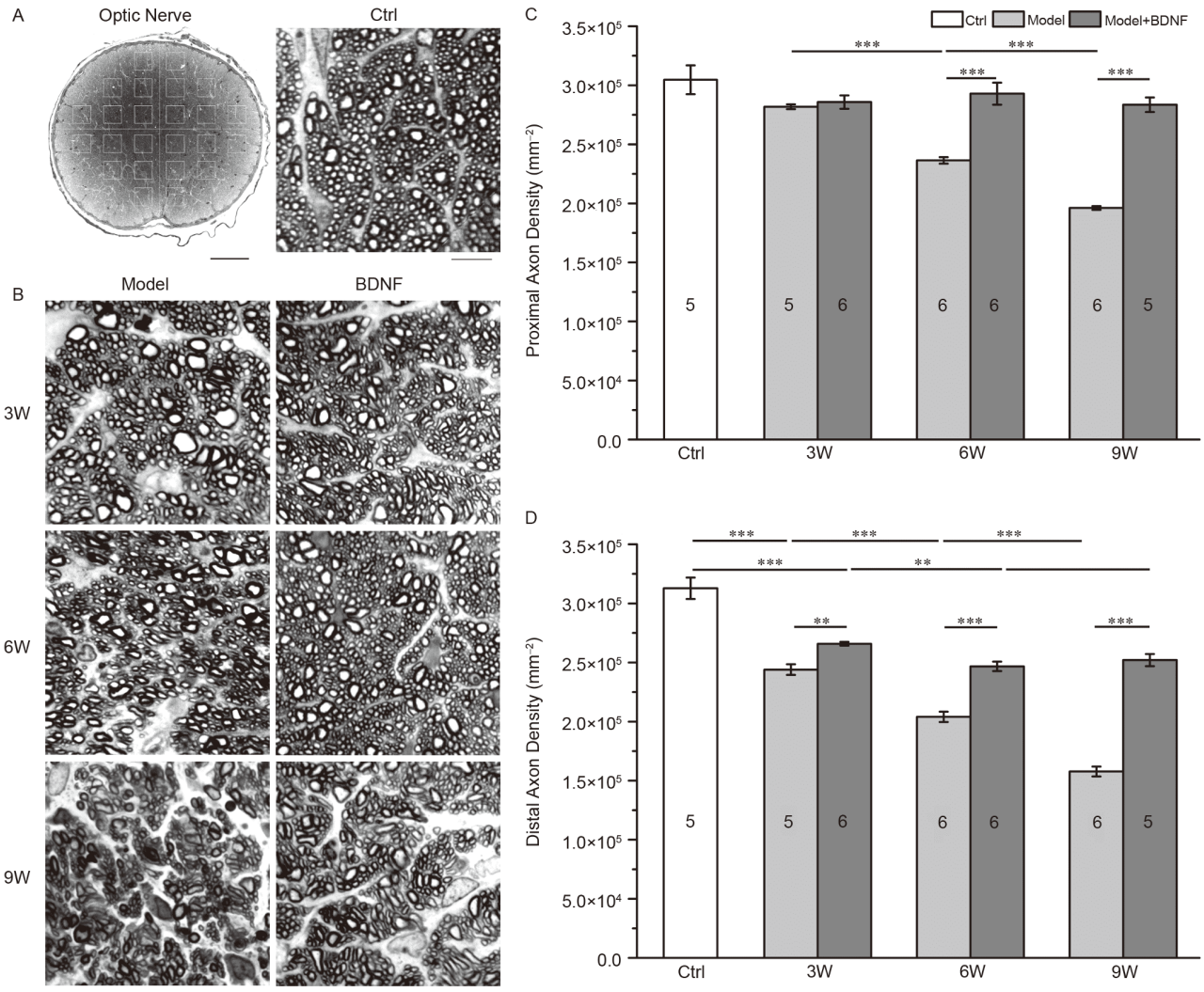

Figure 4 The density of the axons of control, experimental, and BDNF treatment groups. A, An example of a semi-thin resin-embedded cross section of control optic nerve. The 24 white squares shown were counted. Scale bar: 100 μm (left), 10 μm (right). B, Magnifications of the distal optic nerve in acute elevation of IOP and BDNF treatment groups at each time point. The statistics of proximal (C) and distal axons density (D). *, $P<0.05$, **, $P<0.01$, ***, $P<0.001$.

Caution in examining molecular changes

We analyzed molecules involved in axon transportation. The amount of dynein, a motor protein responsible for retrograde transportation (Vale et al., 1985b; Paschal et al., 1987; Schnapp and Reese, 1989) showed a progressive decrease both in the optic nerve and in the retina. BDNF treatment partially restored the decrease, consistent with the impairment and restoration of axon transportation function.

The expression level of kinesin, a motor protein responsible for anterograde transportation (Vale et al., 1985a; Okada et al., 1995; Hirokawa and Noda, 2008) in the optic nerve, exhibited a decrease at the end of 3rd week, and remained quite stable till the end of 9th week, whereas in the retina, the amount exhibited a progressive increase. This result was unexpected. One possible explanation is that the kinesin accumulated in the somas of RGCs with discontinuous axons (Kuribayashi et al., 2010). The difference between continuous (DiD-positive) and physically present axons is the discontinuous axons, correlates with the accumulation of kinesin increased. In the BDNF-treated group, either the reduction in number of disconnected axons or the accumulation of kinesin was no longer significant, although these are only correlations.

The amount of β-tubulin remained unchanged in most cases, both the disease model group and treatment group, exhibited a significant increase in the optic nerve in the very late stage (9th week) of the treatment. In the retina, 60%–70% RGCs may only account for a small proportion of total retinal neurons; it is possible that this change is masked when Western Blotting is performed using the entire retina. However, in the optic nerve, a loss of 30%–50% of axons should be a noticeable difference. It is surprising that the Western Blotting did not detect such a large reduction. Some

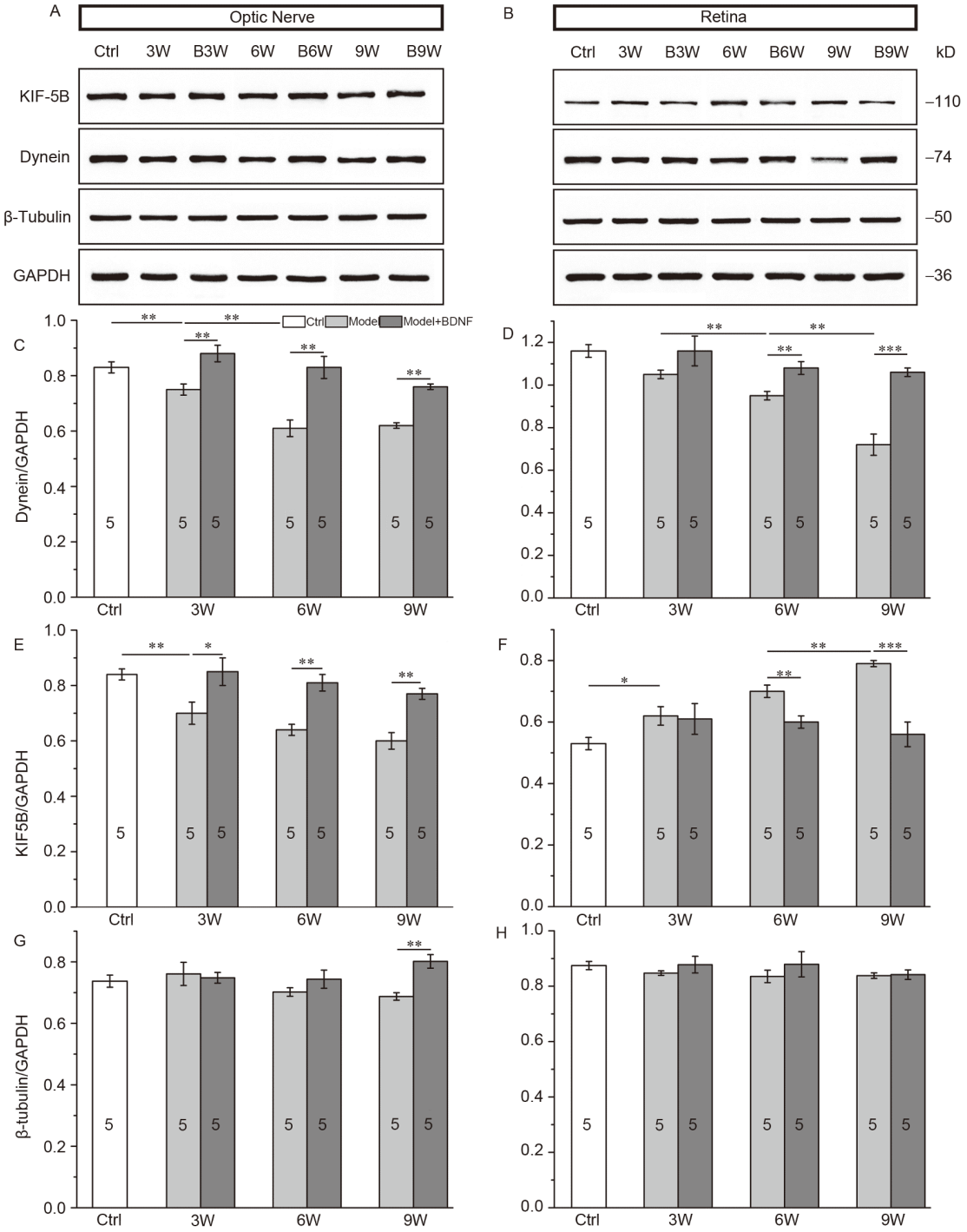

Figure 5 Western Blotting of retina and optic nerve and densitometry analysis. Western Blotting of optic nerve (A) and retina (B) lysates. Densitometry analysis of dynein (C), KIF-5B (E) and β-tubulin (G) in optic nerve. Densitometry analysis of dynein (D), KIF-5B (F) and β-tubulin (H) in retina. *, $P<0.05$, **, $P<0.01$, ***, $P<0.001$.

other unexpected observations, such as a relatively stable area of the optic nerve cross section and an increased number of nuclei in the semi-thin section, led us to look for possible complications. A dramatic gliosis did take place in the degenerating optic nerve, and these findings will be summarized in a separate report. The gliosis may also account for the milder changes of most proteins involved in axon transportation in the optic nerve. Therefore, cautions should be taken in interpreting any data quantifying protein levels in the optic nerve in disease models.

Potential significance

We used an ischemia-reperfusion model (the acute elevation

of IOP) in this study to examine changes in the RGC axons. We found that the axon degeneration in this model is very similar to the degeneration process described in the glaucoma model, but changes occur at a much quicker pace. Future research on similar processes are in the LHON and the ADON, could determine if there is a common target for developing treatments effective for different optic neuropathies.

MATERIALS AND METHODS

Animals

All procedures were in compliance with ARVO Statement for the Use of Animals in Ophthalmic and Vision Research and with the guidelines of Institutional Animal Care and Use Committee of Shanghai Jiao Tong University (Shanghai). Male Sprague-Dawley rats (200–300 g), obtained from the experimental animal center of Shanghai Jiao Tong University (Shanghai), were housed in a 12/12 h light/dark cycle and received food and water *ad libitum*. The number of animals used in each experiment is indicated in the corresponding figure legends or columns.

Rat Acute Elevated IOP

Rat acute elevated IOP was induced (Hughes, 1991). Briefly, the rats were deeply anesthetized with chloral hydrate (400 mg kg^{-1}, Sinopharm Chemical Reagent Co., Ltd, Shanghai) by intraperitoneal injection and topical anesthesia with 0.5% proparacaine hydrochloride eye drops prior to injection. A 29G needle connecting to a reservoir containing sterile saline, was inserted into the anterior chamber of the right eye. IOP was elevated to 130 mmHg for 45 min by raising the reservoir. Retinal ischemia was confirmed by observing whitening of the iris and the retina (Ren et al., 2012).

Intraocular Injection

The procedure used is as described previously (Ren et al., 2012; Cueva Vargas et al., 2016). In brief, 6 h after the acute elevated IOP, BDNF solution (2 μL, 250 ng μL^{-1}, GF029, Millipore, USA) was injected through the sclera into the vitreous humor about 3 mm posterior to the superior-temporal limbus, using a fine glass micropipette. To assess anterograde transportation, rats received an intravitreal injection of 2 μL of 1% cholera toxin subunit B (CTB) conjugated with Alexa Fluor-647 (C34778, invitrogen, USA) as described previously (Crish et al., 2010; Crish et al., 2013; Sun et al., 2011). Care was taken to avoid damage to the lens or vitreous veins during intraocular injection.

Anterograde Transport Measurement

Animals were intracardially perfused with phosphate buffer saline (PBS) followed by 4% paraformaldehyde in PBS 12 h after intraocular CTB injection. Rat brains were removed and cryoprotected in 30% sucrose/PBS overnight. Serial coronal cryosections (15 μm thick) were cut through the entire SC using a cryostat (Leica CM 1950, Germany). From the rostral to caudal SC, a total of 27–35 sections were collected (the first of every four sections). Images were acquired using a Leica confocal microscope equipped with a 10× plan apo objective (NA 0.40, Leica, Germany). Each image of SC (1020×2040 pixels) was vertically divided in to 102 bins (bin width: 20 pixels). The background intensity for each section was calculated by averaging pixels in the nonretinorecipient region of the SC (layers Ⅳ-Ⅶ) or the periaqueductal gray. The contour of the retinorecipient SC was calculated, visually verified and manually adjusted. The pixels with an intensity 2 times above background within the contour were defined as CTB pixels. The ratio of CTB pixels to the total retinorecipient pixels was taken as the bin intensity to construct a colorimetric plot, with 0% being blue and 100% being red. The calculation and construction of the colorimetric plot were carried out using MATLAB R2016b (The MathWorks, Inc., USA).

Double labeling of retinal ganglion cells

To investigate the impairment in retrograde transport function and in axon continuity, we co-injected into the visual tectum a retrograde transported tracer (Vidal-Sanz et al., 1988; Buckingham et al., 2008; Ren et al., 2012), 2% FG (fluorogold, 80014, Biotium, USA) and a lipophilic dye 5% DiD (1, 1′-dioctadecyl-3, 3, 3′, 3′-tetramethylindodicarbocyanine perchlorate, D307, Invitrogen, USA). Briefly, under deep anesthesia, animals were placed on a stereotaxic apparatus (MMN-3, Serial No. 05007, Narishige, Japan). A mixture of DiD and FG were injected into the SC using following coordinates: 5.9 mm posterior to the bregma, 1.0 mm lateral to the midline, and 5.0–4.0 mm deep from the surface of the skull. Animals were allowed to recover in solitary cages and were sacrificed 7 days after injection.

Quantification of RGC somas and axons

Rats were sacrificed by transcardiac perfusion and then fixed with 4% PFA in 0.1 mol L^{-1} PBS; then, retinas were dissected out and fixed for another 30 min. Images were captured from flat-mounted retinas using a laser scanning confocal microscope (TCS-SP8, Leica, Germany). The procedure of analysis of RGC density was performed as previously described (Ren et al., 2012). In brief, using a 20× plan apo objective (NA 0.70, Leica Germany), four images

were captured 500–1,000 μm from the optic disc, and four images were captured 3,000–3,500 μm from the optic disc in each of the four retinal quadrants for a total of 32 retina areas. Images were processed with Image J software (NIH, USA).

For axon counts, animals were sacrificed with a transcardiac perfusion of 0.1 mol L^{-1} PBS then 2% PFA and 2.5% glutaraldehyde in 0.1 mol L^{-1} PBS. RGC axons counted at 2 mm from the optic nerve head were considered as proximal, and 2 mm to optic chiasm were counted as distal. Optic nerves were dissected and fixed in 2% osmium tetroxide, then embedded in epon resin (Electron Microscopy Sciences, USA). Semi-thin cross sections (1.0 μm) were cut on an ultramicrotome (EM UC6, Leica, Germany) and stained with 1% Toluidine Blue. Images were acquired with an epifluorescence microscope (E800, Nikon, Japan) with an oil-immersion 40× plan apo objective (NA 1.0, Nikon, Japan), using a charge-coupled device camera (cascade, Photometrics, USA). A photomontage of the entire optic nerve section was constructed using Photoshop CS6 (Adobe Systems Inc., USA). From the center of the optic nerve, at the interval of 25 μm, six 50×50 μm samples in each quadrant were obtained and counted (Figure 4A). The 24 samples covered a total of 60,000 μm^2 per section (Dai et al., 2012).

Behavioral test of visual function

The apparatus and methods used in this study to measure both visual acuity and contrast sensitivity has been previously described (Prusky et al., 2000; McGill et al., 2004; Ren et al., 2012; Wang et al., 2019). Briefly, a trapezoidal-shaped pool was used, with two monitors placed side-by-side at one end. The pool was filled with 22°C water to a depth of about 15 cm. Visual stimuli (square-wave gratings and uniform gray gratings) were generated and displayed on the monitors using a computer program (Visual Studio 2014, Microsoft, USA). The black level of the screen was 0.05 cd m^{-2} and the white level was 72.8 cd m^{-2}, as measured with a ColorCAL colorimeter (Cambridge Research Systems, UK). A transparent reward platform (37 cm long ×13 cm wide×14 cm high) was hidden under the water below the monitor displaying the grating. The pattern of the grating and platform position was alternated between ends of the pool, with a pseudorandom pattern where no more than three trials were allowed on one side (Gellermann, 1933). All trials were run under dark conditions. The task included three phases: pre-training, task training, and a contrast and acuity test. In the pre-training phase, the rats were trained to swim toward the screen displaying gratings using the visual cues (gratings). In the task training phase, rats were conditioned to swim from a release chute and to associate the platform with the screen displaying gratings using low spatial frequency (0.1 cpd) and high contrast (100%) gratings. Three sessions, of 10 trials per session separated by at least 1 h, were performed in a single day. Once animals achieved 80%+ accuracy in 30 successive trials, the contrast and acuity were measured. In the contrast sensitivity test, the contrast was decreased by 10% each time. In the visual acuity test, the spatial frequency was increased by 0.1 cpd. When the correct rate fell below 70%, the spatial frequency test or contrast sensitivity test were terminated; at that point, measurements were taken as the detection threshold.

Protein extraction and Western Blot analysis

Retinas and optic nerves from each group were homogenized in ice-cold lysis buffer, containing 150 mmol L^{-1} NaCl, 50 mmol L^{-1} Tris, and protease inhibitors. The samples were cleared by centrifugation at 12,100 g for 20 min at 4°C. Protein concentrations were determined using BCA Protein Assay (71285-3, Millipore, USA). Each sample (10 μg) was separated by 10% SDS-PAGE gel, and electrotransferred to a polyvinylidene difluoride membrane (IPVH0010, Millipore, USA). The membrane was blocked with 5% non-fat milk and 0.1% Tween-20 in PBS for 90 min, and was incubated with rabbit anti-KIF5B (1:1,000, Ab167429, Abcam, USA), mouse anti-dynein (1:10,000, MAB1618, Merck Millipore, USA), mouse anti-β tubulin (1:10,000, MAB380, Merck Millipore, USA), and rabbit anti-GAPDH (1:10,000, 2118, Cell Signaling, USA) overnight at 4°C. After 3 washes in Tween/PBS, the membranes were incubated with horseradish peroxidase-conjugated goat anti-mouse IgG (1:10,000, 115-035-003, Jackson ImmunoResearch, USA) and horseradish peroxidase-conjugated goat anti-rabbit IgG (1:10,000, 111-035-003, Jackson ImmunoResearch, USA). Immunopositive bands were revealed with an enhanced chemiluminescence system (WBKL S00 50, Merck Millipore, USA). The scanned film images were analyzed by Image J software and specific band densities were normalized to the band densities of GAPDH.

Statistical analysis

All results are presented as the mean±SE. Statistical analysis was performed using two-sided unpaired student's *t*-test (OriginPro 2016, OriginLab, USA).

Compliance and ethics *All authors certify that they have no affiliations with or involvement in any organization or entity with any financial interest, or non-financial interest, in the subject matter or materials discussed in this manuscript. All procedures performed in studies involving animals were in accordance with the ethical standards of the institution or practice at which the studies were conducted.*

Acknowledgements *This work was supported by The Key Project of National Natural Science Foundation of China (31030036) to Shanghai. We would like to thank Ms. Jiaying Ju for technical support.*

References

Alexander, C., Votruba, M., Pesch, U.E.A., Thiselton, D.L., Mayer, S., Moore, A., Rodriguez, M., Kellner, U., Leo-Kottler, B., Auburger, G., et al. (2000). OPA1, encoding a dynamin-related GTPase, is mutated in autosomal dominant optic atrophy linked to chromosome 3q28. Nat Genet 26, 211–215.

Biousse, V., and Newman, N. (2014). Retinal and optic nerve ischemia. Continuum (Minneap Minn) 20, 838–856.

Buckingham, B.P., Inman, D.M., Lambert, W., Oglesby, E., Calkins, D.J., Steele, M.R., Vetter, M.L., Marsh-Armstrong, N., and Horner, P.J. (2008). Progressive ganglion cell degeneration precedes neuronal loss in a mouse model of glaucoma. J Neurosci 28, 2735–2744.

Cavanagh, J. (1979). The 'dying back' process. A common denominator in many naturally occurring and toxic neuropathies. Arch Pathol Lab Med 103, 659–664.

Coleman, M. (2005). Axon degeneration mechanisms: Commonality amid diversity. Nat Rev Neurosci 6, 889–898.

Crish, S.D., Sappington, R.M., Inman, D.M., Horner, P.J., and Calkins, D.J. (2010). Distal axonopathy with structural persistence in glaucomatous neurodegeneration. Proc Natl Acad Sci USA 107, 5196–5201.

Crish, S.D., Dapper, J.D., MacNamee, S.E., Balaram, P., Sidorova, T.N., Lambert, W.S., and Calkins, D.J. (2013). Failure of axonal transport induces a spatially coincident increase in astrocyte BDNF prior to synapse loss in a central target. Neuroscience 229, 55–70.

Cueva Vargas, J.L., Belforte, N., and Di Polo, A. (2016). The glial cell modulator ibudilast attenuates neuroinflammation and enhances retinal ganglion cell viability in glaucoma through protein kinase A signaling. Neurobiol Dis 93, 156–171.

Dai, C., Khaw, P.T., Yin, Z.Q., Li, D., Raisman, G., and Li, Y. (2012). Structural basis of glaucoma: The fortified astrocytes of the optic nerve head are the target of raised intraocular pressure. Glia 60, 13–28.

Delettre, C., Lenaers, G., Griffoin, J.M., Gigarel, N., Lorenzo, C., Belenguer, P., Pelloquin, L., Grosgeorge, J., Turc-Carel, C., Perret, E., et al. (2000). Nuclear gene OPA1, encoding a mitochondrial dynamin-related protein, is mutated in dominant optic atrophy. Nat Genet 26, 207–210.

Gellermann, L.W. (1933). Chance orders of alternating stimuli in visual discrimination experiments. Pedagog Semin J Genet Psychol 42, 206–208.

Hirokawa, N., and Noda, Y. (2008). Intracellular transport and kinesin superfamily proteins, KIFs: Structure, function, and dynamics. Physiol Rev 88, 1089–1118.

Hoyt, C.S. (1980). Autosomal dominant optic atrophy. Ophthalmology 87, 245–251.

Huang, L., Chen, Y., Lin, Y., Tam, P.O.S., Cheng, Y., Shi, Y., Gong, B., Lu, F., Yang, J., Wang, H., et al. (2019). Genome-wide analysis identified 17 new loci influencing intraocular pressure in Chinese population. Sci China Life Sci 62, 153–164.

Hughes, W.F. (1991). Quantitation of ischemic damage in the rat retina. Exp Eye Res 53, 573–582.

Huoponen, K., Vilkki, J., Aula, P., Nikoskelainen, E. K., Savontaus, M. (1991). A new mtDNA mutation associated with Leber hereditary optic neuroretinopathy. Am J Hum Genet 48, 1147–1153.

Johns, D.R., Neufeld, M.J., and Park, R.D. (1992). An ND-6 mitochondrial DNA mutation associated with Leber hereditary optic neuropathy. Biochem Biophys Res Commun 187, 1551–1557.

Kuribayashi, J., Kitaoka, Y., Munemasa, Y., and Ueno, S. (2010). Kinesin-1 and degenerative changes in optic nerve axons in NMDA-induced neurotoxicity. Brain Res 1362, 133–140.

Liu, L., Li, X., Killer, H.E., Cao, K., Li, J., and Wang, N. (2019). Changes in retinal and choroidal morphology after cerebrospinal fluid pressure reduction: A Beijing iCOP study. Sci China Life Sci 62, 268–271.

Luan, L., Ren, C., Wang, W., Nan, Y., Gao, J., and Pu, M. (2018). Morphological properties of medial amygdala-projecting retinal ganglion cells in the *Mongolian gerbil*. Sci China Life Sci 61, 644–650.

McGill, T.J., Douglas, R.M., Lund, R.D., and Prusky, G.T. (2004). Quantification of spatial vision in the Royal College of Surgeons rat. Invest Ophthalmol Vis Sci 45, 932.

Okada, Y., Yamazaki, H., Sekine-Aizawa, Y., and Hirokawa, N. (1995). The neuron-specific kinesin superfamily protein KIF1A is a uniqye monomeric motor for anterograde axonal transport of synaptic vesicle precursors. Cell 81, 769–780.

Paschal, B.M., Shpetner, H.S., and Vallee, R.B. (1987). MAP 1C is a microtubule-activated ATPase which translocates microtubules *in vitro* and has dynein-like properties. J Cell Biol 105, 1273–1282.

Patel, H.R., and Margo, C.E. (2017). Pathology of ischemic optic neuropathy. Arch Pathol Lab Med 141, 162–166.

Prusky, G.T., West, P.W.R., and Douglas, R.M. (2000). Behavioral assessment of visual acuity in mice and rats. Vision Res 40, 2201–2209.

Qiao, L., Zhang, X., Jan, C., Li, X., Li, M., and Wang, H. (2019). Macular retinal thickness and flow density change by optical coherence tomography angiography after posterior scleral reinforcement. Sci China Life Sci 62, 930–936.

Quigley, H.A., Addicks, E.M., and Green, W.R. (1982). Optic nerve damage in human glaucoma. Arch Ophthalmol 100, 135.

Reichstein, D., Ren, L., Filippopoulos, T., Mittag, T., and Danias, J. (2007). Apoptotic retinal ganglion cell death in the DBA/2 mouse model of glaucoma. Exp Eye Res 84, 13–21.

Ren, R., Li, Y., Liu, Z., Liu, K., and He, S. (2012). Long-term rescue of rat retinal ganglion cells and visual function by AAV-mediated BDNF expression after acute elevation of intraocular pressure. Invest Ophthalmol Vis Sci 53, 1003–1011.

Sadun, A. A., Win, P. H., Ross-Cisneros, F., Walker, S., Carelli, V. (2000). Leber's hereditary optic neuropathy differentially affects smaller axons in the optic nerve. Trans Am Ophthalmol Soc 98, 223–235.

Schnapp, B.J., and Reese, T.S. (1989). Dynein is the motor for retrograde axonal transport of organelles. Proc Natl Acad Sci USA 86, 1548–1552.

Sun, L., Han, X., and He, S. (2011). Direction-selective circuitry in rat retina develops independently of GABAergic, cholinergic and action potential activity. PLoS ONE 6, e19477.

Vale, R.D., Reese, T.S., and Sheetz, M.P. (1985a). Identification of a novel force-generating protein, kinesin, involved in microtubule-based motility. Cell 42, 39–50.

Vale, R.D., Schnapp, B.J., Mitchison, T., Steuer, E., Reese, T.S., and Sheetz, M.P. (1985b). Different axoplasmic proteins generate movement in opposite directions along microtubules *in vitro*. Cell 43, 623–632.

Vidal-Sanz, M., Villegas-Pérez, M.P., Bray, G.M., and Aguayo, A.J. (1988). Persistent retrograde labeling of adult rat retinal ganglion cells with the carbocyanine dye dil. Exp Neurol 102, 92–101.

Votruba, M., Fitzke, F.W., Holder, G.E., Carter, A., Bhattacharya, S.S., and Moore, A.T. (1998). Clinical features in affected individuals from 21 pedigrees with dominant optic atrophy. Arch Ophthalmol 116, 351–358.

Wallace, D.C., Singh, G., Lott, M.T., Hodge, J.A., Schurr, T.G., Lezza, A. M., Elsas, L.J., and Nikoskelainen, E.K. (1988). Mitochondrial DNA mutation associated with Leber's hereditary optic neuropathy. Science 242, 1427–1430.

Wang, W., Nan, Y., Pan, Z.H., and Pu, M. (2017). Morphological evaluation of retinal ganglion cells expressing the L132C/T159C ChR2 mutant transgene in young adult cynomolgus monkeys. Sci China Life Sci 60, 1157–1167.

Wang, X., Shen, K., Lu, F., and He, S. (2019). Long-lasting impairments in rodent oxygen-induced retinopathy measured by retinal vessel density and visual function. Sci China Life Sci 62, 681–690.

Weinreb, R.N., Aung, T., and Medeiros, F.A. (2014). The pathophysiology and treatment of glaucoma: A review. JAMA 311, 1901–1911.

Whitmore, A.V., Libby, R.T., and John, S.W.M. (2005). Glaucoma: Thinking in new ways—A role for autonomous axonal self-destruction and other compartmentalised processes? Prog Retinal Eye Res 24, 639–662.

Xia, H., Hu, Q., Li, L., Tang, X., Zou, J., Huang, L., and Li, X. (2019).

Protective effects of autophagy against blue light-induced retinal degeneration in aged mice. Sci China Life Sci 62, 244–256.
Xin, C., Tian, N., Li, M., Wang, H., and Wang, N. (2018). Mechanism of the reconstruction of aqueous outflow drainage. Sci China Life Sci 61, 534–540.
Yohannan, J., and Boland, M.V. (2017). The evolving role of the relationship between optic nerve structure and function in glaucoma. Ophthalmology 124, S66–S70.
Zhang, J., Jia, H., Wang, J., Xiong, Y., Li, J., Li, X., Zhao, J., Zhang, X., You, Q., Zhu, G., et al. (2019). A novel deletion mutation, c.1296delT in the BCOR gene, is associated with oculo-facio-cardio-dental syndrome. Sci China Life Sci 62, 119–125.
Zhang, X., Yuan, Q., and Gao, X. (2018). Assessment of the MT1-MMP expression level of different cell lines by the naked eye. Sci China Life Sci 61, 492–500.
Zhou, Y., Xiao, C., and Pu, M. (2017). High glucose levels impact visual response properties of retinal ganglion cells in C57 mice—An *in vitro* physiological study. Sci China Life Sci 60, 1428–1435.

SUPPORTING INFORMATION

Figure S1 The trends for visual acuity and contrast threshold.

Figure S2 6 h, 12 h, and 24 h of the CTB signal density in the superior colliculus.

Figure S3 The pathology of the proximal and middle optic nerve.

The supporting information is available online at http://life.scichina.com and https://link.springer.com. The supporting materials are published as submitted, without typesetting or editing. The responsibility for scientific accuracy and content remains entirely with the authors.